Plasmon assisted Nd^{3+} based solid-state nanolaser

Pablo Molina,[1] Eduardo Yraola,[1] Mariola O. Ramírez,[1] Christos Tserkezis,[2] José L. Plaza,[1] Javier Aizpurua,[2] Jorge Bravo-Abad[3] and Luisa E. Bausá[1]*

[1]Dept. Física de Materiales and Instituto Nicolás Cabrera, Universidad Autónoma de Madrid, 28049-Madrid, Spain

[2]Center for Materials Physics (CSIC-UPV/EHU) and Donostia International Physics Center (DIPC), Paseo Manuel Lardizabal 4, 20018-Donostia-San Sebastián, Spain

[3]Dept. Física Teórica de la Materia Condensada and Condensed Matter Physics Center (IFIMAC), Universidad Autónoma de Madrid, 28049-Madrid, Spain

ABSTRACT - Solid-state lasers constitute essential tools in a variety of scientific and technological areas, being available in many different designs. However, although nanolasing has been successfully achieved for dyes and semiconductor gain media associated with plasmonic structures, the operation of solid-state lasers beyond the diffraction limit has not been reported yet. Here we demonstrate room temperature laser action with sub-wavelength confinement in a Nd^{3+}-based solid-state laser by means of the localized surface plasmon resonances supported by chains of metallic nanoparticles. We show a 50% reduction of the pump power at threshold and a remarkable 15-fold improvement of the slope efficiency with respect to the bulk laser operation. The results can be extended to the large diversity of solid-state lasers with the subsequent impact on their applications.

KEYWORDS: Nd^{3+}, plasmonic nanolaser, solid-state laser, chains of Ag nanoparticles

Since the first experimental demonstration of the ruby laser in 1960,[1] the development of solid-state lasers (SSLs) has led to an enormous variety of systems capable of generating laser action with characteristics relevant for applications in research, industry, medicine or optical communications.[2] Their versatile performance includes the possibility of operating in continuous-wave or ultra-short pulsed regimes, as well as single line or tunable sources,[3-5] being accessible in very different configurations comprising from large devices delivering high power to fibers or compact microchip lasers for integrated optics.[6-8] In this class of lasers, the laser transition usually takes place between localized crystal-field levels of rare-earth or transition-metal ions incorporated as optically active impurities in insulating crystals, glasses or ceramics.[9] Additionally, an external optical resonator containing the gain medium is generally employed to provide the optical feedback. Among the different optically active ions, trivalent neodymium (Nd^{3+}) is by far the most widely employed laser ion due to its excellent properties. Namely, it shows a four-level operation in pulsed or continuous-wave (cw) mode, presents a metastable laser level of high quantum efficiency, and has numerous absorption bands throughout the visible and the near-infrared (NIR) spectral regions to ensure efficient pumping.[9]

In the last years, nanoscale laser action with sub-diffraction confinement has been reported for a certain number of configurations combining different gain media (mainly organic dye molecules or semiconductors) with plasmonic nanostructures.[10-18] However, although plentiful devices allow shaping the spatial, temporal and spectral profile of SSLs, laser operation from these systems at the nanoscale remains a challenge.

Here we report on the first demonstration of a SSL operating at the subwavelength scale. The system operates at room temperature with a laser emission wavelength close to 1 μm. As gain

medium we have used a Nd^{3+} doped periodically poled $LiNbO_3$ (Nd^{3+}:PPLN) laser crystal,[19] on which long chains of closely spaced silver interacting nanoparticles (NPs) have been deposited (Figure 1a). These chains were assembled on the ferroelectric domain boundary surfaces of the PPLN laser crystal following a simple and low-cost photochemical procedure.[20] The chain length was around 2 mm. The average size of the silver NPs was about 50 nm and the average inter-particle distance close to 2 nm (See Supporting Information and Figure 1b). The metallic nanostructures support broad radiative plasmonic modes which extend from the visible down to the NIR matching the relevant optical transitions of Nd^{3+} ions.[21] Indeed, the possibility to boost the Nd^{3+} photoluminescence in this class of system has been recently reported.[21,22]

To evaluate the effect of the Ag NP chains on the laser performance of our system, we carried out spatially resolved scanning confocal laser gain microscopy experiments (Figure 1a). We pump the device along the *c*-optical axis of the crystal by means of a cw Ti:sapphire laser tuned at 808 nm, where the maximum of the $^4I_{9/2} \rightarrow {}^4F_{5/2}$ absorption of Nd^{3+} ions in $LiNbO_3$ takes place.[23] After a fast non radiative decay to the $^4F_{3/2}$ upper metastable state, radiative transitions to the lower lying states take place. Out of these transitions, free running laser occurs in a four level scheme at the $^4F_{3/2} \rightarrow {}^4I_{11/2}$ (~1μm) transition (Figure 1c).

For a pump beam polarized parallel to the Ag NP chains (with powers in the 125-300 mW range), full laser oscillation occurs only at the immediate surroundings of the metallic nanostructures. The stimulated emission takes place for the individual $^4F_{3/2}(R_1) \rightarrow {}^4I_{11/2}(Y_3)$ Stark transition at λ_e=1093 nm, the spectral linewidth being 0.6 cm^{-1}, which corresponds to the limit of our experimental set-up (green curve in Figure 2a). A two dimensional spatial map of the integrated laser intensity is depicted in Figure 2b. The image replicates the periodicity of the

plasmonic arrays (Figure 2c) and is consistent with a nanoscale confinement driven by the localized surface plasmon (LSP) resonances supported by the metallic NP chains. This sub-wavelength confinement can be achieved all along the chain. The spatial distribution of lasing confirms the nanoscopic character of the laser action around the plasmonic nanostructures and reveals a significant threshold reduction with respect to the bare Nd^{3+}:$LiNbO_3$ regions. A discussion on the extent of the improvement of the laser threshold for the plasmon-assisted geometry is given in the Supporting Information.

As it generally occurs in SSLs, due to the high reflectance of the mirrors forming the Fabry-Pérot resonator, the evolution from spontaneous emission to laser action cannot be monitored. Accordingly, Figure 3b shows the input-output gain curves obtained from the laser light emitted in the vicinity of the metallic nanostructures for two polarization states of the pump beam, parallel and perpendicular to the chains (Figure 3a). As expected, they display the pronounced threshold behavior characteristic of SSLs. Depending on the polarization of the pump beam, we observe two different threshold values, the lowest being obtained when the pump beam is polarized parallel to the NPs chains. The laser slope efficiency is similar for both pump polarizations, parallel and perpendicular. According to the C_3 symmetry site of Nd^{3+} ions in $LiNbO_3$ and to the forced electric-dipole character of the Stark transitions in this system,[24] the intensity of the optical transitions of Nd^{3+} ions does not vary when rotating the polarization around the *c*-optical axis of the crystal. The significant threshold reduction when pumping parallel to the chains can thus be accounted for in term of the nanophotonic properties of the metallic NP chains as we will be discussed below.

On the other hand, the laser preferentially oscillates perpendicularly to the domain walls on which the metallic NPs are deposited. This also occurs in the absence of NPs, and relates to the effect of light diffraction at the ferroelectric domain boundaries, which affects more intensely to the light polarized parallel to the boundaries.[25] As a result, the cavity losses increase preventing laser oscillation with this polarization. Note that although laser action occurs at the nanoscale, the emitted radiation travels in the resonator through the whole thickness of the medium.

The observed plasmon-mediated lasing process at the nanoscale can be well compared with the conventional bulk laser operation obtained in the same Nd^{3+}:$LiNbO_3$ gain medium in the absence of metallic NP chains and under the same experimental configuration. In this case the laser exhibits a pump power at threshold two times larger than that observed for lasing around the plasmonic chains (parallel pump beam). We also observe a remarkable deterioration of the laser slope efficiency (by a factor of 15) as a result of the bulk photorefractive effect in $LiNbO_3$.[19] The significant threshold reduction when pumping parallel to the chains is enabled by both the cross-section of the system and the significant field confinement close to the surface of the considered crystal. The latter effect allows overcoming the well-known nonlinear instabilities that characterize the bulk configuration of this class of solid-state lasers (namely, the photorefractive damage[19]), and observe stable laser action at the power levels reported in this work.

To obtain further physical insight into the experimental observations, we carried out full-wave simulations of the near-field response of the metallic NP chain deposited on top of a Nd^{3+}:PPLN laser crystal (see supporting information). Figure 3c displays cross sections of the electric-field distribution at the NP midplane computed at the pump wavevelength λ_a=808 nm, as obtained for

an incident plane wave polarized along the direction of the metallic NP chain (top) and perpendicularly to it (bottom). Similar mode profiles were obtained at the laser emission wavelength λ_e=1093 nm (not shown). For incident polarization parallel to the chain, the optical pump excites a plasmonic resonance characterized by a large electric-field enhancement (of about a factor 100) in the air gap in-between the NPs.[26] This enhancement is significantly reduced (to a factor of approximately 5) when the system is illuminated by a pump perpendicularly polarized with respect to the chain. To reveal the effect of the plasmonic local fields on the lasing action, we develop a simple semi-analytical model.[27,28] Within this approach, the lasing threshold (R_p^{th}) and slope efficiency (G_e), derived from the dependence of the photon-number on the external pump rate, can be written as $R_p^{th} = V_a / (Q_e \Gamma \zeta)$ and $G_e = Q_e / \omega_e$. V_a stands for the volume of the laser medium, whereas the parameter ζ includes the details of the laser transition (see supporting information). The photonic temporal and spatial confinement properties of the system at the lasing frequency are accounted for by the corresponding quality factor (Q_e) and energy confinement factor (Γ), respectively. Taking into account that the laser photons generated by both polarizations of the pump are stored in the same lasing mode (the plasmonic mode that starts lasing first), the laser slope efficiency is independent of the polarization of the pump field, and governed by the product ΓQ_e (Figure 3d). This result agrees well with the fact that similar slope efficiencies are obtained experimentally for the two polarizations of the pump beam (Figure 3b). On the other hand, from our numerical calculations we obtained quality factors of $Q_a \approx 4$ and $Q_a \approx 1$ for the modes excited at λ_a=808 nm with parallel and perpendicular pump polarizations, respectively. Thus, the larger photon-lifetime τ_a associated with the plasmonic mode excited at λ_a by the parallel polarization (note that

$\tau_a = Q_a \lambda_a / 2\pi c$) leads to a reduction of the corresponding value of R_p^{th} with respect to the perpendicular polarization. From this argument it follows that the parallel polarization is expected to feature a lasing threshold approximately a factor of 4 smaller than that corresponding to the perpendicular polarization (Figure 3d). We believe that the discrepancy between the experimental and theoretical results can be ascribed to larger scattering losses (which leads to a smaller value of Q_a) present in the experimental system, mainly due to disorder and dispersion in size of the NPs. Overall, the tendencies and values derived from our theoretical analysis support the mechanism of plasmonic light-trapping as the mediator of the nanoscale lasing action in our system.

In summary, we have demonstrated room temperature laser operation of a Nd^{3+} based SSL at the nanoscale by exploiting the capability of LSPs from linear chains of metallic NPs. Our results unambiguously show that laser action occurs in a nanometric region of the system in which the pump power at threshold features a dramatic reduction compared to the conventional bulk laser operation in the same system. These findings open up the fascinating possibility of extending the approach reported here to the extremely vast list of solid state gain media, constituted by hundreds of host-ion combinations. This novel class of plasmonic lasers could cover a broad spectral range from the ultraviolet to the mid-infrared, with the inherent advantages of compactness, chemical and thermal frequency stability distinctive of SSLs, and with the subsequent significant impact for the development of a wide variety of devices and applications.

SUPPORTING INFORMATION AVAILABLE

Experimental section; details on the numerical calculations; analysis on the extent of improvement of the laser threshold for the plasmon-assisted geometry including the calculated scattering cross section of chains with different number of NPs. This material is available free of charge via the Internet at http://pubs.acs.org

AUTHOR INFORMATION

Corresponding Author

*Email: luisa.bausa@uam.es

Author Contributions

P.M., E.Y, M.O.R. and L.E.B. were in charge of the experimental results. C.T., J.A. and J.B.-A. worked on the theoretical analysis. J.L.P. performed the crystal growth. M.O.R., J.B.-A. and L.E.B. wrote the manuscript. L.E.B. conceived the project and supervised the work. All authors contributed to the scientific discussion.

Note: The authors declare no competing financial interest.

ACKNOWLEDGMENT

This work has been supported by the Spanish Ministry of Economy and Competitiveness (MINECO) under projects MAT2013-43301-R and FIS2013-41184-P and Comunidad de Madrid under grant S2013/MIT-2740.

REFERENCES

(1) Maiman, T. H. *Nature* **1960**, 187, 493-494.

(2) Denker, B., Shklovsky, E. Eds.; *Handbook of Solid-State Lasers: Materials, Systems and Applications*; Woodhead Publishing, Cambridge, 2013.

(3) Sennaroglu, A. *Handbook of Solid-State Lasers and Applications*; CRC Press, Boca Raton, 2007.

(4) Keller, U. *Nature* **2003**, 424, 831-838.

(5) Kaminskii, A. A. *Laser Crystals: Their Physics and Properties*; Springer Verlag, Berlin, 1990.

(6) Perry, M. D.; Mourou, G. *Science* **1994**, 264, 917-924.

(7) Jackson, S. D. *Nature Photon*. **2012**, 6, 423-431.

(8) Zayhowski, J. J.; Mooradian, A. *Opt. Lett.* **1989**, 14, 24-26.

(9) Huber, G.; Krankel, C.; Petermann, K. *J. Opt. Soc. Am. B* **2010**, 27, 93-105.

(10) Oulton, R.F.; Sorger, V.J. ; Zentgraf, T.; Ma, R.M.; Gladden, C.; Dai, L.; Bartal, G.; Zhang, X. *Nature* **2009**, 461, 629-632.

(11) Hill, M.T.; Marell, M.; Leong, E.S.P.; Smalbrugge, B.; Zhu, Y.C.; Sun, M.H.; van Veldhoven, P.J.; Geluk, E.J.; Karouta, F.; Oei, Y.S. *Opt. Express* **2009**, 17, 11107-11112.

(12) Noginov, M. A.; Zhu, G.; Belgrave, A. M.; Bakker, R.; Shalaev, V. M.; Narimanov, E. E.; Stout, S.; Herz, E.; Suteewong, T.; Wiesner, U. *Nature* **2009**, 460, 1110.

(13) Ma, R.M.; Oulton, R.F.; Sorger, V.J.; Bartal, G.; Zhang, X.A. *Nature Mater.* **2011**, 10, 110-113.

(14) Lu, Y. J.; Kim, J.; Chen, H.-Y.; Wu, C.; Dabidian, N.; Sanders, C. E.; Wang, C. Y.; Lu, M.-Y.; Li, B. H.; Qiu, X.; Chang, W.-H.; Chen, L. J.; Shvets, G.; Shih, C. K.; Gwo, S. *Science* **2012**, 337, 450−453.

(15) Wu, X. ; Xiao, Y.; Meng, C.; Zhang, X. ; Yu, S.; Wang, Y.; Yang, C.; Guo, X.; Ning, C. Z.; Tong, L. *Nano Lett.* **2013**, 13, 5654–5659.

(16) Zhou, W.; Dridi, M.; Suh, J. Y.; Kim, C. H.; Co, D. T.; Wasielewski, M. R.; Schatz, G. C.; Odom, T. W. *Nat. Nanotechnol.* **2013**, 8, 506−511.

(17) Lu, Y. J.; Wang, C. Y.; Kim, J.; Chen, H. Y.; Lu, M. Y.; Chen, Y. C. l; Chang, W. H.; Chen, L. J.; Stockman, M. I.; Shih, C. K.; Gwo, S. *Nano Lett.* **2014**, 14, 4381-4388.

(18) Sidiropoulos, T.P.H.; Roder, R.; Geburt, S.; Hess, O.; Maier, S.A.; Ronning, C.; Oulton, R.F. *Nature Phys.* **2014**, 10, 870-876.

(19) Fan, T. Y.; Cordova-Plaza, A.; Digonnet, M. J. F.; Byer, R. L.; Shaw, H. J. *J. Opt. Soc. Am. B* **1986**, 3, 140-148.

(20) Kalinin, S. V.; Bonnell, D. A.; Alvarez, T.; Lei, X. J.; Hu, Z. H.; Shao, R.; Ferris, J. H. *Adv. Mater*. **2004**, 16, 795.

(21) Yraola, E.; Molina, P.; Plaza, J. L.; Ramirez, M. O.; Bausa, L. E. *Adv. Mater.* **2013**, 25, 910-915.

(22) Molina, P.; Yraola, E.; Ramirez, M. O.; Plaza, J. L.; De las Heras, C.; Bausa, L. E. *Nano Lett.* **2013**, 13, 4931-4936.

(23) Burlot, R.; Moncorge, R.; Manaa, H.; Boulon, G.; Guyot, Y.; Sole, J. G.; Cochet, M., D. *Opt. Mater.* **1996**, 6, 313−330.

(24) Bonardi, C; Carvalho, R.A.; Basso, H.C.; Terrile, M.C.; Cruz, G.K.; Bausa, L.E.; Sole, J.G. *J. Chem. Phys.* **1999**, 111, 6042-6046.

(25) Müller, M., Soergel, E., Wengler, M.C.; Buse, K. **2004**, 78, 367-370.

(26) Maier, S. A. *Plasmonics: Fundamentals and Applications*; Springer, New York, 2007.

(27) Chang, S. W.; Chuang, S. L. *IEEE J. Quantum Electron.* **2009**, 45, 1004-1013.

(28) Cuerda, J., Ruting, F., Garcia-Vidal, F. J.; Bravo-Abad, J. *Phys. Rev. B* **2015**, 91, 5.

Figure 1

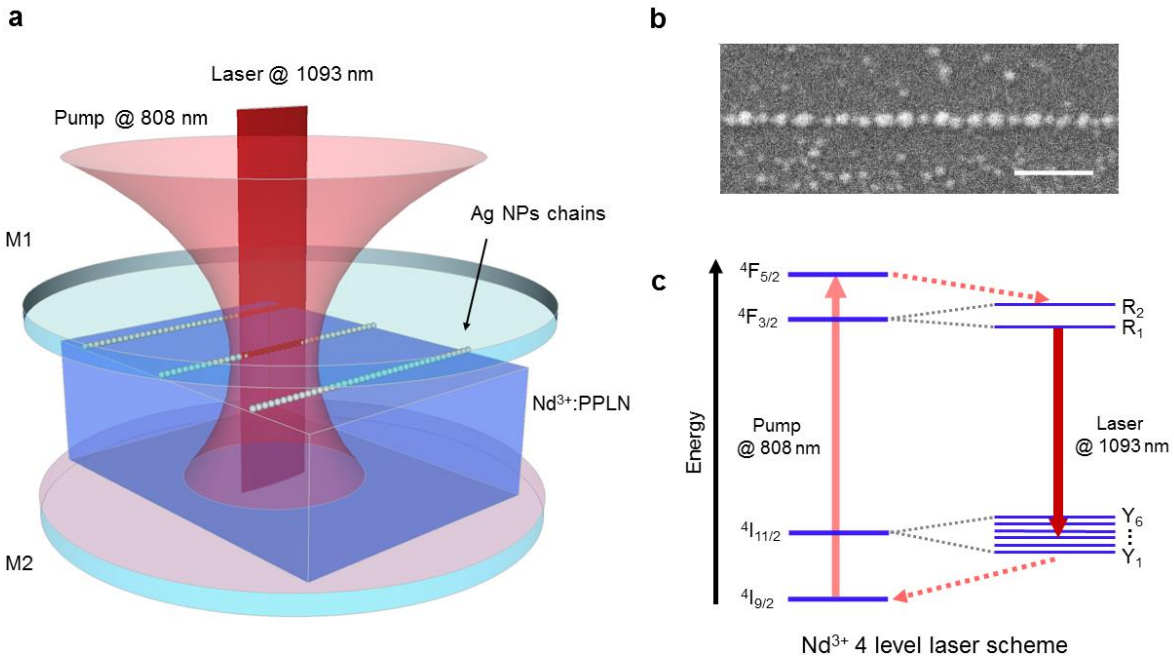

Figure 1. (a) Schematics of the optically pumped Nd^{3+} based solid-state nanolaser. A Nd^{3+}:PPLN solid-state gain medium with periodical arrays of Ag NP chains deposited on it is placed between two plane-parallel mirrors (Fabry-Pérot resonator). The system is optically pumped at λ_a=808 nm with a 20x microscope objective, and the generated laser radiation at λ_e=1093 nm is collected by the same objective in backscattering geometry. (b) SEM image showing a portion of a chain of Ag NPs deposited onto the domain wall surface of the crystal. Scale bar corresponds to 200 nm. (c) Energy level diagram of Nd^{3+} displaying the pump and laser transitions and the crystal field splitting of the relevant $^4F_{3/2}$ and the $^4I_{11/2}$ states. The Stark transition for which laser action is obtained in this work ($R_1 \rightarrow Y_3$) has been highlighted by a thick arrow.

Figure 2

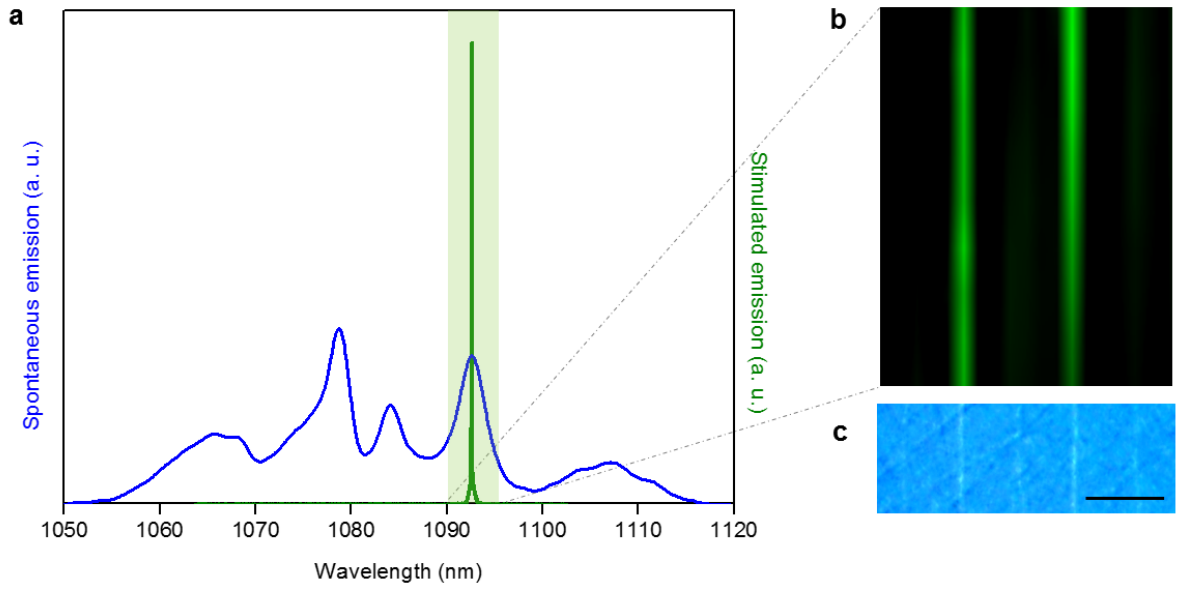

Figure 2. (a) Spontaneous and stimulated emission spectra corresponding to the $^4F_{3/2} \rightarrow {}^4I_{11/2}$ transition of Nd^{3+} in $LiNbO_3$. The spontaneous emission spectrum shows a clear structure due to the Stark splitting of the involved states by the effect of the crystal field (blue line). The stimulated emission spectrum corresponds to the individual $^4F_{3/2}(R_1) \rightarrow {}^4I_{11/2}(Y_3)$ Stark transition at λ_e=1093 nm (green line). (b) Spatially resolved confocal laser gain image obtained by integrating the laser intensity when the pump radiation (fixed at a power of 230 mW) is scanned on a macroscopic area containing several chains. (c) Detailed view of an optical micrograph of the crystal surface around the Ag NP chains. Scale bar corresponds to 5 μm. Laser oscillation takes place in the vicinity of the chains while it is absent in the remaining areas.

Figure 3

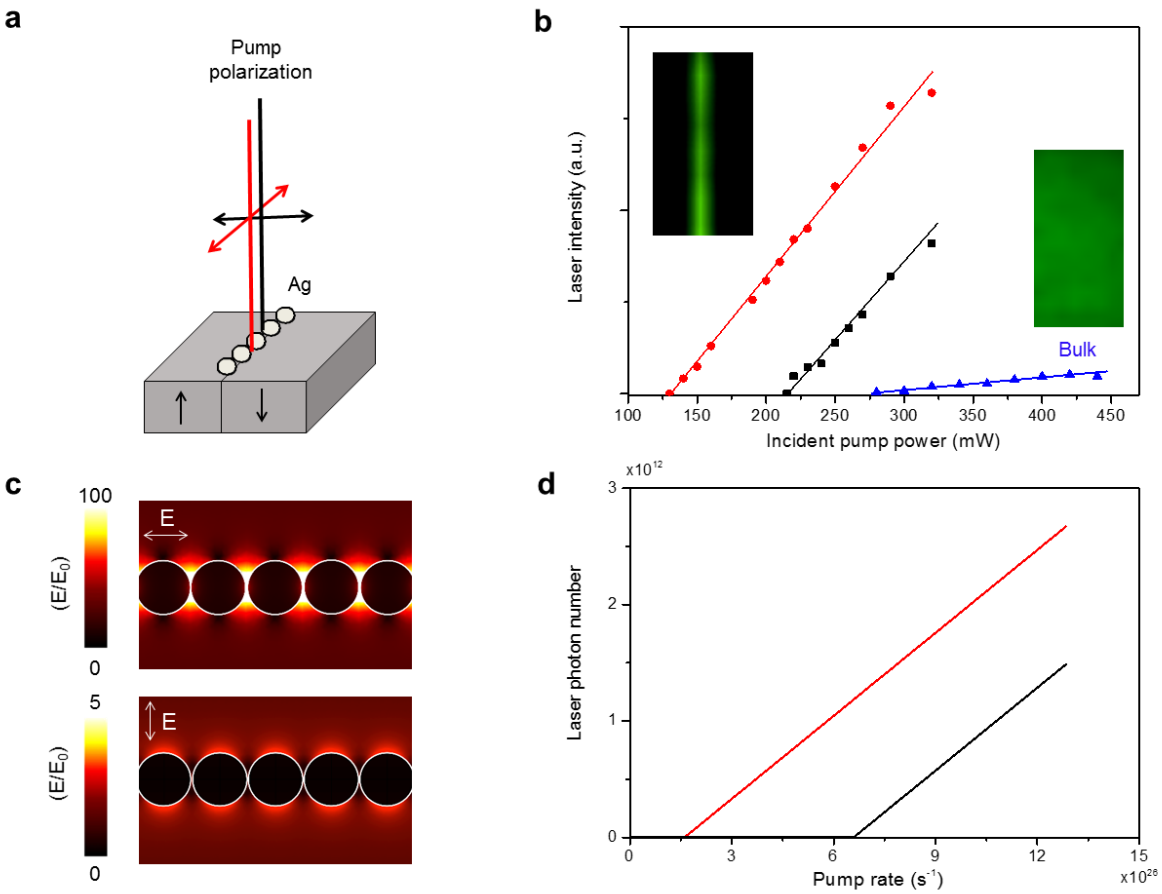

Figure 3. (a) Schematics of the pump configuration of the plasmon mediated Nd^{3+}:PPLN laser crystal (b) Input-output laser gain curves at the vicinity of the Ag NP chains when the pump beam is polarized parallel (red) and perpendicular to the chains (black). The lowest threshold value is obtained when the pump beam is polarized parallel to the chains. The laser performance of the same Nd^{3+}:PPLN crystal after removing the chains (bulk behavior) is shown in blue. In this case the spatial distribution of the laser intensity presents a homogeneous distribution (right inset) in contrast to the well-defined line pattern obtained around the metallic nanostructures (left inset). For illustrative purposes the image from the non-plasmonic part of the gain medium has

been multiplied by a factor of 15. (c) Calculated electric-field amplitudes of the plasmonic resonances excited at λ_a=808 nm using parallel and perpendicular incident polarizations (top and bottom panels, respectively). In both cases, the displayed cross-section corresponds to a xy plane (parallel to the $LiNbO_3$ surface) passing through the center of the Ag NP chain. (d) Calculated steady-state values of the laser photon-number as a function of the pump rate for the case of parallel (red line) and perpendicular (black line) pump polarizations.